(Received 14 July 2025, Accepted 20 November 2025, Scheduled 14 December 2025)

Metasurface-Driven Improvement in MIMO Antenna Performance by Addressing Mutual Coupling

Safia Jaouad[1,*], Chaymae Chahboun[1], Mohammed A. Ennasar[1], Otman EL Mrabet[1], Jesús R. Perez[2], Mohsine Khalladi[1], and Mariem Aznabet[1]

[1] *Intellegent System Design Laboratory (ISD), Faculty of Science, Abdelmalek Essaadi University, Tetouan, Morocco*
[2] *Departamento de Ingeniería de Comunicaciones, Universidad de Cantabria, Santander, Spain*

ABSTRACT: In this paper, a metasurface is proposed as an effective solution to enhance the performance of MIMO antennas by reducing mutual coupling. This reduction is attributed to the metasurface's negative permeability at the resonant frequency, which helps to block waves propagating between the two adjacent structures. The designed metasurface consists of a 2D array of omega-shaped resonators placed over two linearly polarized patch antennas. Measurement results show a 15 dB reduction in coupling when the metasurface is positioned $0.14\lambda_0$ above two closely spaced antennas separated by $0.06\lambda_0$ at a resonant frequency of 2.85 GHz. Additionally, improvements in other characteristics of the whole structure, such as gain and radiation efficiency, were also observed. Such an achievement has not been reported in the literature on previous metasurface-based decoupling methods. This technique can be useful for massive multiple input multiple output (mMIMO) systems for wireless communications.

1. INTRODUCTION

Multiple-input multiple-output (MIMO) systems are defined as those in which both transmitting and receiving ends have multiple antenna elements. Multiple antennas significantly improve channel capacity, spectral efficiency, and fading reduction without requiring more bandwidth or transmission power [1]. As a result, MIMO technology is expected to be used in wireless communication networks in the most recent wireless devices. A distance of at least $0.5\lambda_0$ (where λ_0 is the free space wavelength at the working frequency) is required between antenna elements for low correlation and adequate isolation [2]. In practical applications such as 5G devices, the space available for implementing MIMO antennas is limited. Consequently, the separation distance between antennas is less than $0.2\lambda_0$, which leads to the occurrence of mutual coupling between antennas. This coupling degrades the performance of MIMO antennas [3, 4]. To address this issue, mutual coupling must be either eliminated or significantly reduced. Up to now, various decoupling techniques [5, 6] have gained attention, going beyond merely increasing the physical separation between elements. Traditional approaches, such as electromagnetic bandgap (EBG) structures [7], defected ground structures (DGSs) [8], metamaterial structures [9], and decoupling networks [10], have been proposed to achieve high isolation performance. All these mentioned decoupling techniques require additional physical space between antennas, which can be a significant drawback for systems where miniaturization is critical. Additionally, most of these techniques are not easily scalable to massive MIMO antenna arrays with dozens of elements.

Recently, metasurfaces have been explored as a cutting-edge solution for reducing decoupling between antenna elements. In [5, 6], a suspended metasurface is introduced to decouple a MIMO array. This metasurface is designed to reject unwanted radiation and reduce mutual coupling in the antenna array without affecting other performance aspects. Additionally, another low-profile decoupling method is presented in [7], utilizing metamaterial structures integrated into the same layer as the coupled array. This metasurface, also composed of periodic square split ring resonators (SRRs), manipulates electromagnetic waves to effectively demonstrate its decoupling effects. In [11], a metasurface is placed above two dielectric resonator antennas to reduce the mutual coupling between the elements. More recently, Tang et al. [12] proposed a multi-frequency MIMO antenna based on a metasurface for 5G and WiFi-6E applications. The design employs SRRs and a spiral metasurface to achieve tri-band operation around 3.5, 5.8, and 6.9 GHz while effectively reducing surface and space-wave coupling. Measurements demonstrated high isolation (up to ∼36 dB), improved gain and efficiency, and very low ECC, confirming the effectiveness of the metasurface approach.

While the above cited works focus exclusively on linearly polarized MIMO antenna systems, Wu and Yan [13] extended the concept to circularly polarized arrays. They introduced a metasurface with periodic Jerusalem cross-slots to decouple a 2×2 CP microstrip array, reporting significant reductions in mutual coupling (24 dB and 16 dB in the E- and H-planes, respectively) and a gain improvement of ∼1.5 dBi. Another important work that deals with CP MIMO antennas is reported in [14]. The authors design a metasurface augmented CP MIMO antenna operating across multiple frequency bands.

* Corresponding author: Safia Jaouad (safia.jaouad@gmail.com).

Metasurface is used to mitigate both surface-wave and space-wave coupling among antenna elements, resulting in a significant improvement in isolation with only minimal degradation of gain. Their experimental results confirm that integrating a metasurface can preserve overall performance while reducing coupling effectively.

This paper introduces a novel low-profile metasurface decoupling method. The proposed structure consists of a metasurface made up of omega-shaped resonators (OSRs), positioned near a two-element coupled antenna array. The structure was fabricated and tested, with results demonstrating that the metasurface significantly enhances isolation performance. Additionally, other characteristics, such as gain and radiation efficiency, were improved. To the best of the authors' knowledge, such an achievement has not been reported in the literature on previous metasurface-based decoupling methods.

2. MECHANISM OF DECOUPLING USING A NEGATIVE PERMEABILITY METASURFACE

2.1. Decoupling Mechanism

It is well known that as the distance between antennas decreases, mutual coupling increases, which progressively degrades the antenna's performance. To mitigate the coupling, metasurfaces can be used. This approach involves placing a metasurface above two coupled antenna elements to enhance decoupling. The metasurface consists of periodic unit cells, each functioning as a magnetic resonator. The decoupling mechanism is based on the specific properties of these unit cells, particularly the complex wave number, which plays a critical role in controlling electromagnetic interactions. These resonators are designed to exhibit tailored resonance frequencies and strong field confinement, ensuring effective decoupling and optimizing performance. Fig. 1 illustrates the radiated field distributions of a two-coupled MIMO antenna system with the introduction of the metasurface. The aim of the metasurface is to enhance the isolation between the antennas by absorbing the waves radiated by Antenna 1 to couple to Antenna 2 (terminated with a 50-Ω load). This can be explained by the fact that the metasurface exhibits both a negative permeability and a positive permittivity around the same resonance frequency of the excited antenna. Then, the complex wavenumber, which can be calculated using the following equation $k = k_0\sqrt{|\varepsilon_r|\,|\mu_r|}$,

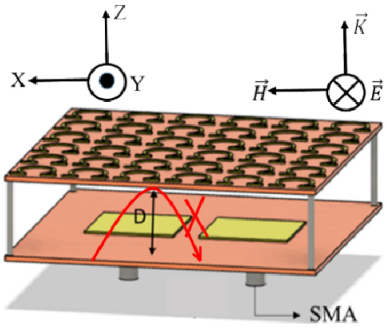

FIGURE 1. The principle of the proposed decoupled array with the omega-shaped metasurface.

becomes purely imaginary $k = jk_0\sqrt{|\varepsilon_r|\,|\mu_r|}$ in the case of $\mu_r < 0$ and $\varepsilon_r > 0$. Now, the x-component of the electric field propagating in the $-x$ direction, A_0e^{jkx}, can take the following form:

$$A_0e^{jkx}A_0e^{j\omega t} = A_0e^{j(jk_0\sqrt{|\varepsilon_r||\mu_r|}x)}e^{j\omega t} \tag{1}$$

From (1), we can clearly see that the electromagnetic wave traveling in the x-direction of the omega-shaped metasurface is evanescent. This ensures that the mutual coupling between the two antennas is eliminated. When the wave emitted by the antennas propagates along the z-direction, with the magnetic field component aligned in the x-direction, radiation is guaranteed due to the metasurface's anisotropic characteristics [15].

2.2. Proposed Configuration for Enhancing Decoupling

The configuration of the proposed high isolation MIMO antenna based on a metasurface with a negative permeability is depicted in Fig. 2. It consists of two closely spaced rectangular patches coupled in the H-plane and separated from edge-to-edge by a distance of $d = 0.06\lambda_0$ which is 7 mm at the resonant frequency of 2.85 GHz. Both rectangular patches have identical dimensions and are placed below a metasurface with negative permeability that acts as a superstrate and is securely held in place by four acrylic screws, ensuring a proper alignment. The rectangular patches, fed by a 50-Ω coaxial probe, are printed on a grounded dielectric substrate (Rogers RT/Duroid 4003C) with a permittivity of 3.55, a loss tangent of 0.0027, and a thickness of $h_1 = 1.524$ mm. The metasurface is placed at a distance D of 30 mm (about 0.14λ at 2.85 GHz) above the antenna to reduce the mutual coupling between both antennas. The metasurface is a 2-D array consisting of 6×6 elements and has the same aperture area as the radiating patch's substrate, $67.4 \times 67.4\,\text{mm}^2$. Each element of the metasurface consists of an omega-shaped resonator (OSR). The proposed structure is designed and optimized using commercial software, the full-wave simulation software CST Microwave Studio. The optimized dimensions

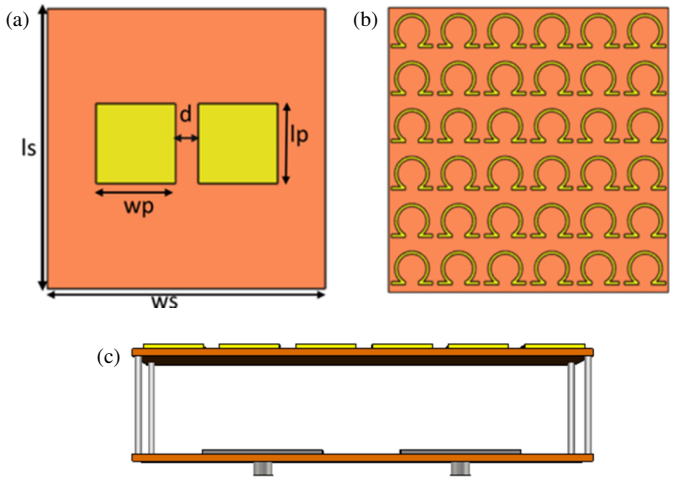

FIGURE 2. Antenna structure. (a) The antenna array without metasurface, (b) the metasurface layer, and (c) the side view of the antenna array with metasurface.

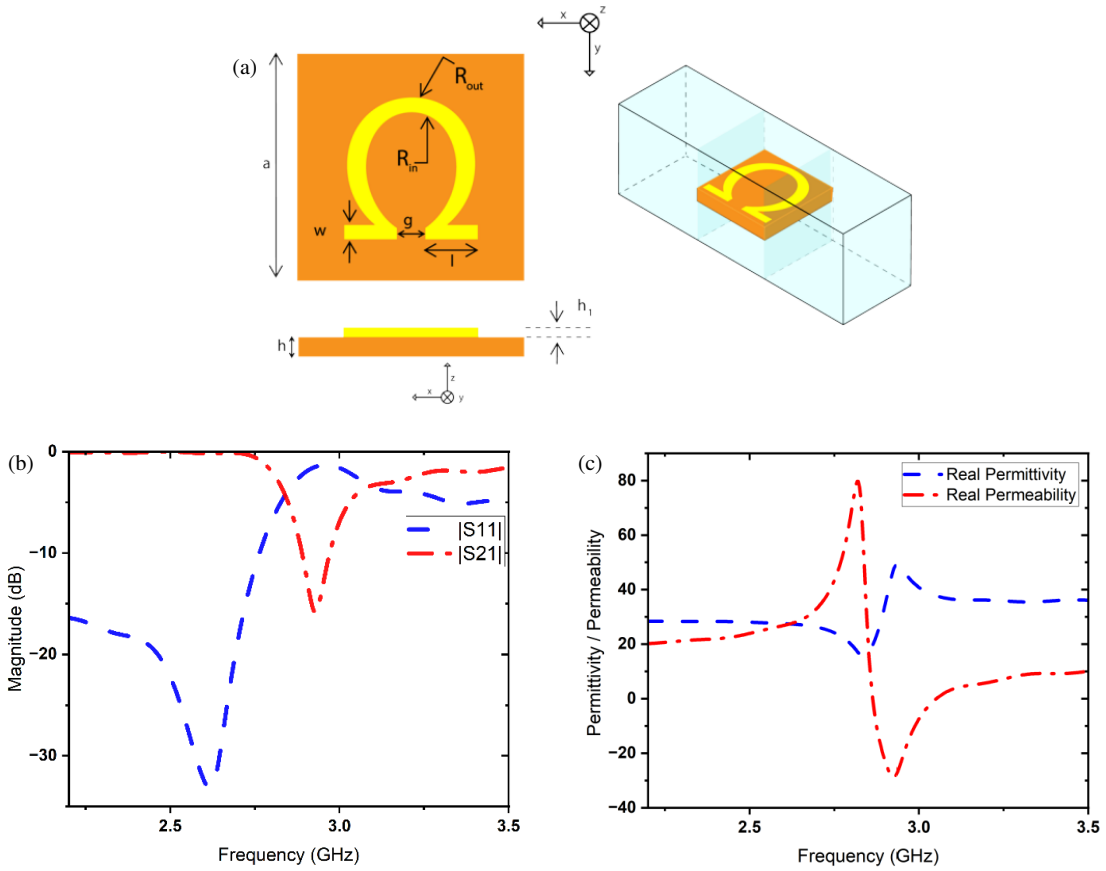

FIGURE 3. The unit cell design. (a) Layout of the omega-shape resonator elements. (b) S-parameter of the unit cell. (c) Permittivity and permeability.

of the rectangular patch are as follows: $W_S = L_S = 112\,\text{mm}$, $W_P = 26.8\,\text{mm}$, $L_P = 26.66\,\text{mm}$.

2.3. Effective Parameters of the OSR Unit Cell

The design procedure started with calculating the effective parameters of the metasurface, especially permittivity and permeability. The omega-shaped metasurface unit cell was modeled using CST Microwave Studio and tuned to achieve a negative permeability (MNG), which means has a magnetic resonator around the resonance frequency of 2.85 GHz. The main parameters of the OSR are listed in Table 1. The simulation setup used is depicted in Fig. 3(a). To simulate a periodic array of OSRs placed in the x-y plane (Fig. 3(b)), a single OSR unit cell is simulated with PEC and PMC boundary conditions, which are defined in such a way that the magnetic field is kept along x. In contrast, the electric field is kept along the y-axis. Consequently, the propagation direction of the wave vector k is in the z direction. From the obtained simulated S parameters of the unit cell (S_{11} and S_{21}), the effective parameters were calculated using the retrieval method developed in [16]. Fig. 3(c) shows the effective parameters (ε_r and μ_r) of the metasurface as a function of the frequency. It can be observed that the permeability μ is negative around the resonance frequency 2.85 GHz, which is exploited to build a superstrate for eliminating the coupling between the two-element antenna array.

TABLE 1. Parameters of the omega-shape unit (Unit: mm).

Parameter	Value	Parameter	Value
a	16.35	g	4.5
r_{in}	5	r_{out}	6
h	1.524	h_1	0.035
w	1.1	l	5

2.4. Simulated Results and Parametric Study

Figure 4 shows the simulated S-parameters with and without the metasurface. Note that the metasurface is placed 2 mm above the 2-port antennas. It can be seen clearly that the $-10\,\text{dB}$ impedance bandwidth without metasurface is 2.8% (2.8–2.88 GHz), whereas that of the one with metasurface is 5.9% (2.82–3 GHz). In contrast, the MIMO antenna without a metasurface experiences significant mutual coupling, with an S_{21} of $-8\,\text{dB}$ at 2.85 GHz. However, with the integration of the metasurface, the mutual coupling is significantly reduced to $-22\,\text{dB}$, while the maximum isolation improves to 56 dB at 2.9 GHz, demonstrating outstanding decoupling performance. The OSR metasurface effectively blocks coupling between the two elements of the antenna array, significantly reducing interference. When loaded with a negative permeability medium (metasurface) that acts as an evanescent medium in the x-direction, further minimizing unwanted coupling between the

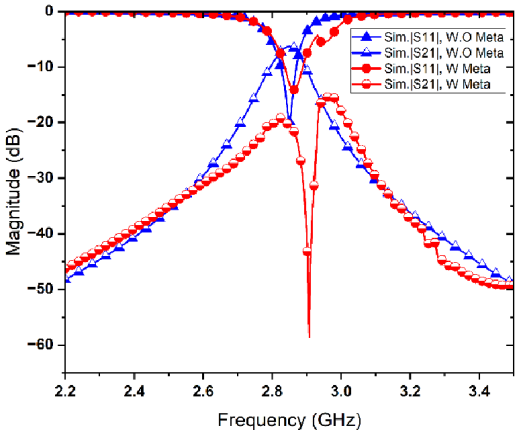

FIGURE 4. Simulated S-parameter of an antenna array without and with metasurface.

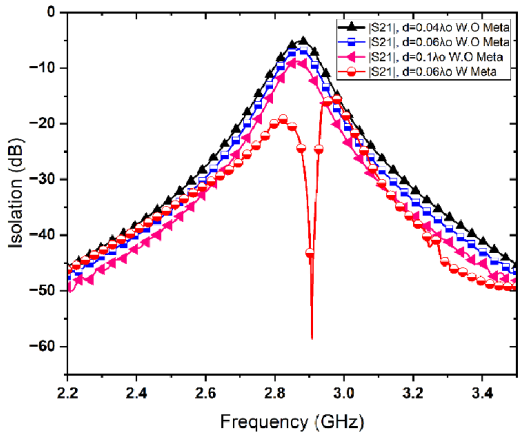

FIGURE 5. Simulated isolations for arrays with different d values without a metasurface and the isolation for the array with a metasurface.

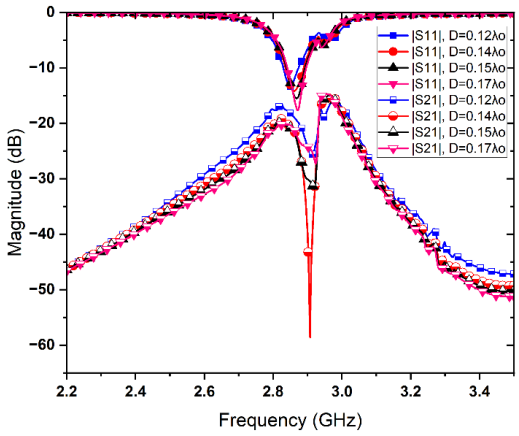

FIGURE 6. Simulated S-parameters of the array with the metasurface concerning different D.

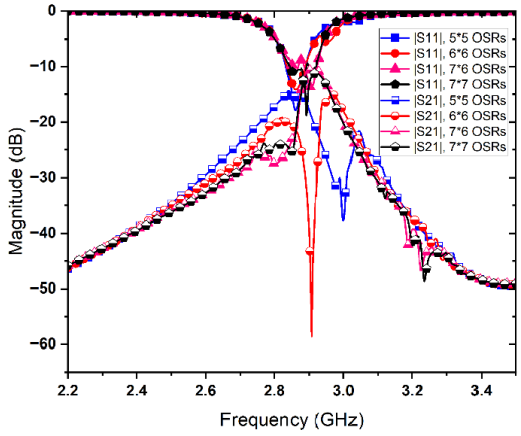

FIGURE 7. Simulated S-parameters of the antenna array with the metasurface for a different number of OSR units.

antenna elements, the small increase in bandwidth can be attributed to the presence of the metasurface near the antenna, which alters its radiation resistance and reactive impedance. This effectively acts as a design element that lowers the quality factor and enhances impedance matching, thereby broadening the antenna bandwidth. It is worth noting that a greater increase in bandwidth could be achieved by increasing the separation distance between the radiating elements and the metasurface.

However, this paper's primary objective is to reduce mutual coupling. Nonetheless, the slight enhancement in bandwidth could be interesting in some applications. This technique's main advantage is its ability to decrease the separation distance between antennas in MIMO antenna systems, enabling a more compact design.

Reducing the system size makes it suitable for applications with stringent space constraints. Additionally, this compact configuration can enhance system integration and contribute to reducing material costs. Furthermore, due to the necessity of placing a metasurface closely over the radiating elements, the structure remains a low-profile design, as the spacing between the metasurface and the MIMO antenna system is small $(0.06\lambda_0)$.

Next, we have performed many full-wave simulations to analyze the effect of key design features on the performance of the proposed design, with a particular focus on its impedance characteristics (S_{11} and S_{21}). We note that while varying a single parameter, the remaining feature dimensions were kept at their previously optimized values.

The first parameter examined in this study is the separation distance (d) between two adjacent antennas as depicted in Fig. 5. The miniaturization of antenna array elements, particularly reducing the spacing between them, is critical for various applications, including MIMO systems. Typically, a separation distance of $\lambda_0/2$ is required to minimize mutual coupling. However, in the design proposed, different values of d have been considered to achieve a more compact configuration. The obtained results are plotted in Fig. 5. From this figure, it can be inferred clearly that the reflection coefficient (S_{11}) remains relatively insensitive to variations in the separation distance (d). However, the transmission coefficient (S_{21}) exhibits significant changes with the parameter d. Notably, optimal decoupling performance is achieved at a spacing of $d = 0.06\lambda_0$.

In addition to the effect of element spacing, d, the effect of the separation distance between the antenna and the metasurface

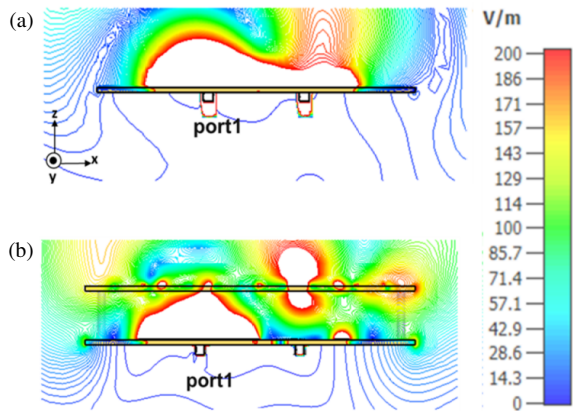

FIGURE 8. Simulated electric field distribution on the XOZ-plane cutting surface when Antenna 1 is excited and Antenna 2 is terminated with a 50-Ω matched load, shown for: (a) the array without, and (b) with the metasurface, respectively.

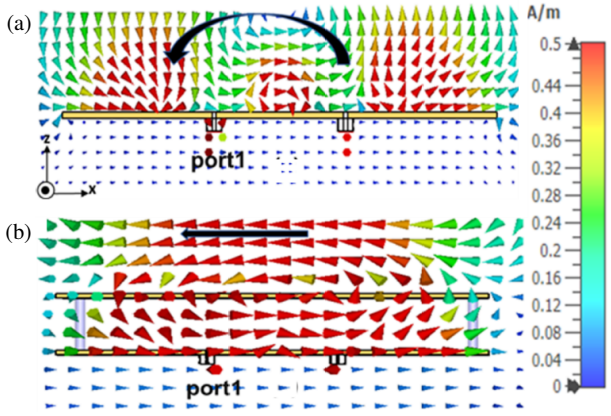

FIGURE 9. Simulated magnetic field distribution on the XOZ-plane cutting surface when Antenna 1 is excited and Antenna 2 is terminated with a 50-Ω matched load, shown for: (a) the array without, and (b) with the metasurface, respectively.

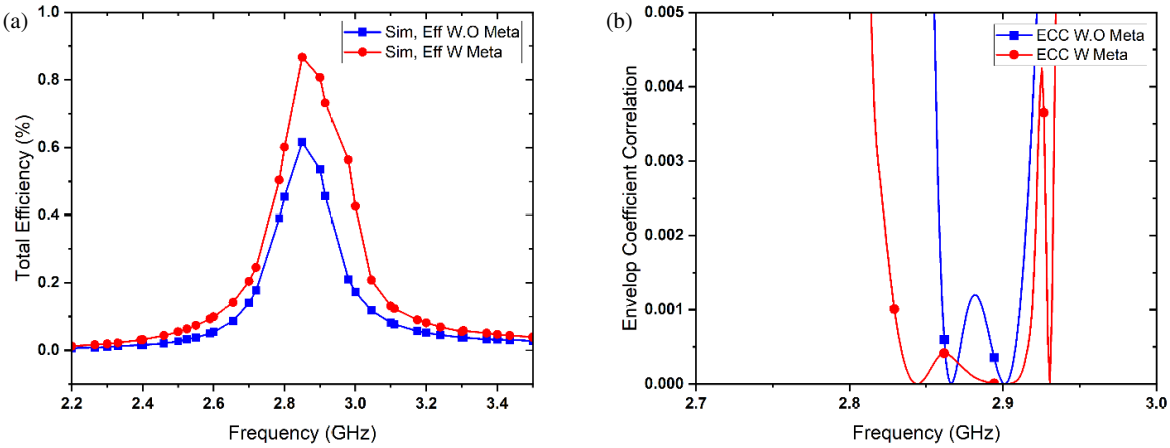

FIGURE 10. Efficiency and ECC values. (a) Simulated radiation efficiency. (b) Simulated envelope correlation coefficient (ECC).

(D) is also studied, as shown in Fig. 6. It is evident that the optimal value of D for achieving a good isolation is $0.14\lambda_0$.

Finally, the effect of the number of unit cells of the metasurface is examined in Fig. 7. It is observed that varying the number of unit cells significantly impacts both the reflection coefficient (S_{11}) and the transmission coefficient (S_{21}). The 5×5 unit cell configuration exhibits the same isolation as the 6×6 unit cell configuration, but with a greater bandwidth of 3.2 GHz compared to 2.88 GHz for the latter. The 6×6 and 7×7 unit cell configurations provide a broader bandwidth compared to the others. Thus, the OSR metasurface can also enhance the bandwidth with an optimal number of unit cells. As previously mentioned, the primary objective of this work is to enhance the mutual coupling performance of the proposed structure. The best configuration to achieve this within the band of interest is the 6×6 unit cell configuration.

To explore the decoupling mechanism further, Fig. 8 compares the simulated electric field distributions with and without the metasurface. In the simulation, Antenna 1 is excited while Antenna 2 is terminated with a 50-Ω matched load. From Fig. 8, it can be observed that in the absence of the metasurface, stray coupling from Antenna 1 is transferred to Antenna 2 and absorbed by the load. However, with the introduction of the metasurface, the wavefront is effectively focused toward the normal direction of Antenna 1.

This can be explained by the fact that the energy flow generated by Antenna 1 is canceled by the metasurface, which produces an opposing energy flow, thereby reducing the coupling strength between the two antennas. Furthermore, as shown in Fig. 9, the metasurface is composed of omega-shaped resonators that act as magnetic resonators. The comparison of the simulated magnetic field distribution with and without the metasurface reveals that the magnetic field produced by the metasurface propagates predominantly along the negative x-axis.

This opposing magnetic field interacts with the field from the antennas, thereby suppressing a significant portion of the mutual coupling between them in the MIMO system.

Following this, the radiation efficiency and envelope correlation coefficient (ECC) are also studied numerically and presented in Fig. 10. It can be seen from this figure that loading both antennas with the metasurface increase the radiation effi-

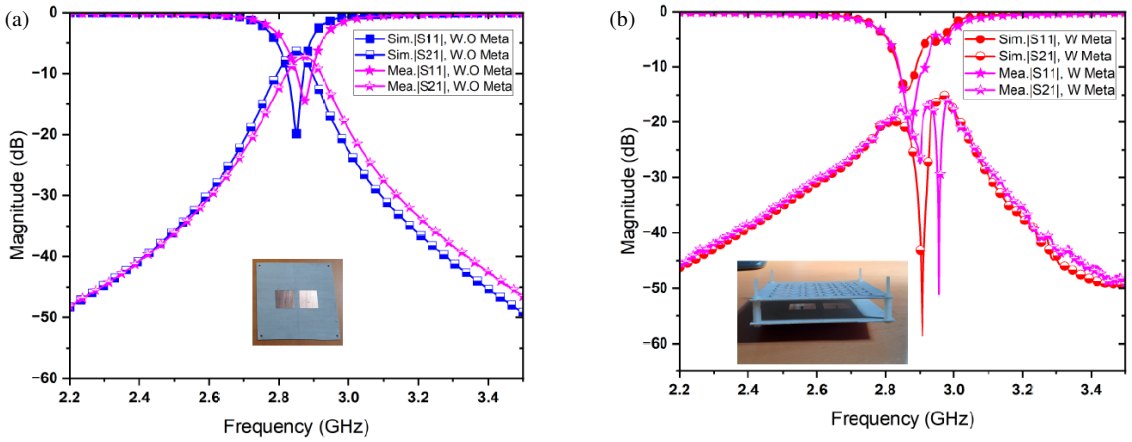

FIGURE 11. Simulated and measured S-parameters of the antenna structure: (a) without, and (b) with the metasurface.

ciency from 66% to 90%, representing a 24% improvement, and significantly lowers the ECC at the operating frequency from 0.01 to 0.0001. Reducing the value of ECC improves the system's diversity gain, increases channel capacity, and enhances spectral efficiency, leading to better overall MIMO performance.

For channel capacity loss (CCL), there exists a direct relationship with ECC. Indeed, CCL is derived from the same correlation matrix that already includes ECC. Therefore, when the ECC values are extremely low (≈ 0), as observed in our design (0.0001), the CCL becomes negligible (close to 0 bits/s/Hz). This demonstrates that very low ECC obtained not only validates excellent diversity gain but also guarantees minimal capacity loss, which implies that the value of CCL in this case is expected to be very small.

Another important factor in evaluating MIMO system performance is diversity gain (DG), which reflects the reliability of the system. A higher diversity gain indicates improved isolation and better diversity performance, and it depends on the correlation coefficients between the antenna signals. For the proposed design, the calculated ECC is 0.001, which yields a DG of 9.99 dB according to expression (2), indicating an almost ideal performance.

$$\mathrm{DG} = 10 \times \sqrt{1 - \mathrm{ECC}} \tag{2}$$

3. RESULTS AND DISCUSSION

To validate our approach, a prototype was fabricated and tested using a Keysight N5234B vector network analyzer (Fig. 15(a)). Fig. 11(a) shows the S-parameters of the proposed antenna structure without the metasurface, and Fig. 11(b) shows the antenna with the metasurface. There is a strong agreement observed between the measured and simulated results. The measured operating bandwidth for the antenna without the metasurface, with $|S_{11}| < -10$ dB, is around 45 MHz, and $|S_{21}|$ is approximately 6 dB. However, for the case of the antenna structure with metasurface, the measured coupling achieves a level of more than 40 dB at 2.8–2.9 GHz as the metasurface is placed above the antenna at a distance of $D = 0.14\lambda_0$, with a significantly increased bandwidth.

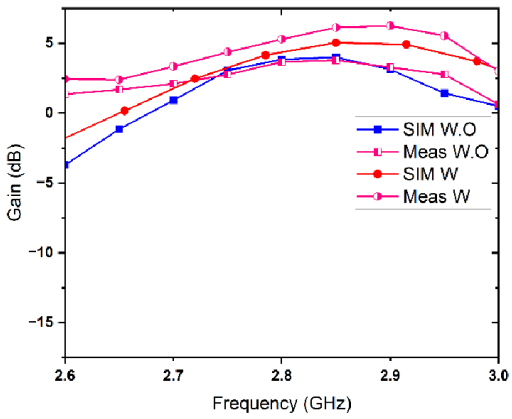

FIGURE 12. Gain of the antenna array without and with the metasurface when Antenna 1 is excited and Antenna 2 is terminated with a 50-Ω matched load.

It is important to note that the coupling can be decomposed into lateral (surface-wave-driven currents that flow along the array plane) and radiated (space-wave) power normal to the array. Our metasurface is designed to suppress the lateral component by enforcing an MNG regime (high surface impedance), thereby minimizing surface currents between elements; most of the energy is redirected into radiation rather than lateral transport, which aligns with the observed drop in the coupling parameter S_{21}. The observed frequency shift (Fig. 11(b)) is attributed to the metasurface's non-flat placement over the antenna structure or to manufacturing tolerances. These promising results validate the effectiveness of the proposed decoupling method based on the use of a metasurface with negative permeability.

Next, we have measured the realized gain and radiations patterns using an ultra-wideband (UWB) time-domain measurement kit (Geozondas), as illustrated in Fig. 15(b). The setup operates in the time domain, employing sub-nanosecond impulse signals and wideband horn antennas as transmit/receive probes. The time-domain response is then Fourier-transformed to extract the radiation characteristics over the desired frequency range, enabling fast and accurate far-field pattern measurements without the need for frequency-by-frequency sweeps.

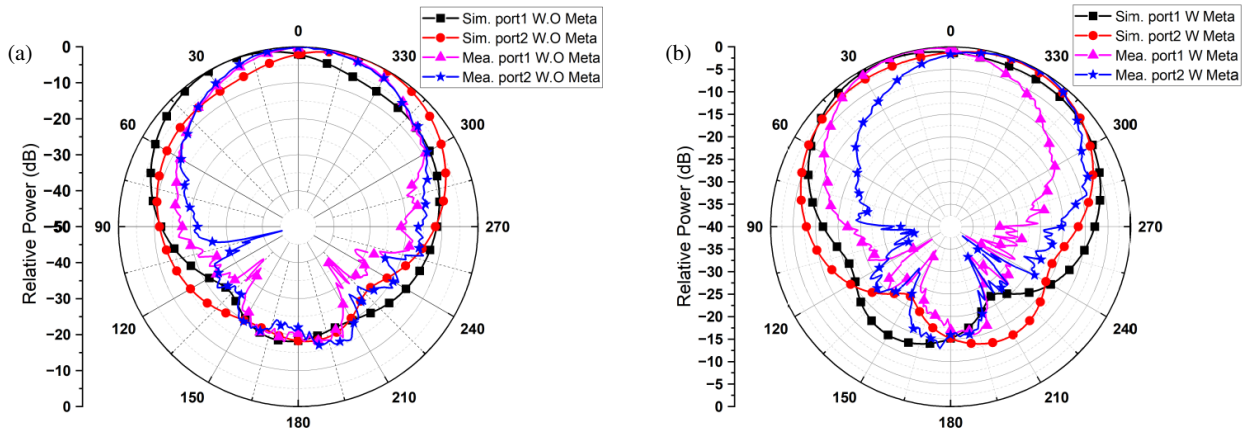

FIGURE 13. Simulated and measured radiation patterns of the array antenna at 2.85 GHz for the H-plane: (a) without, (b) with metasurface.

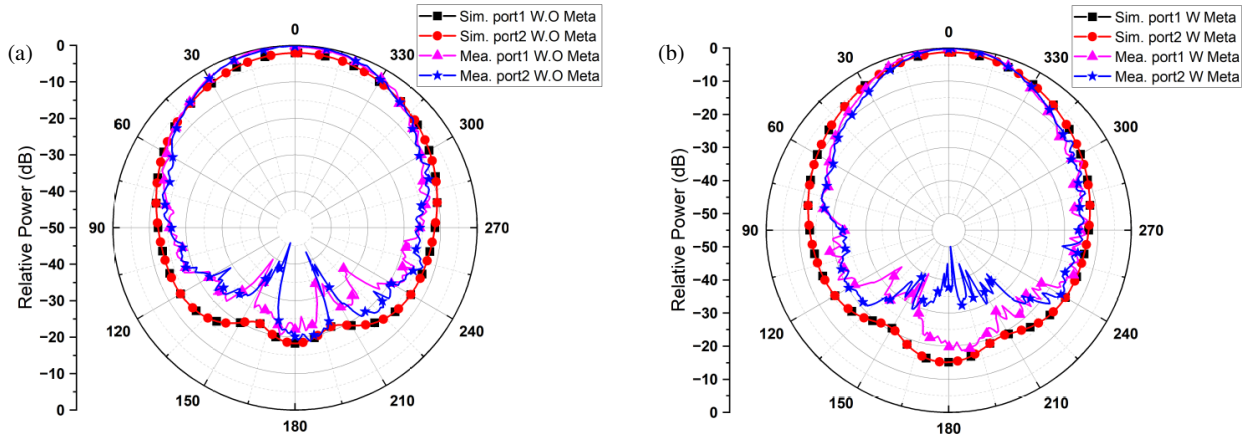

FIGURE 14. Simulated and measured radiation patterns of the array antenna at 2.85 GHz for the E-plane: (a) without, (b) with metasurface.

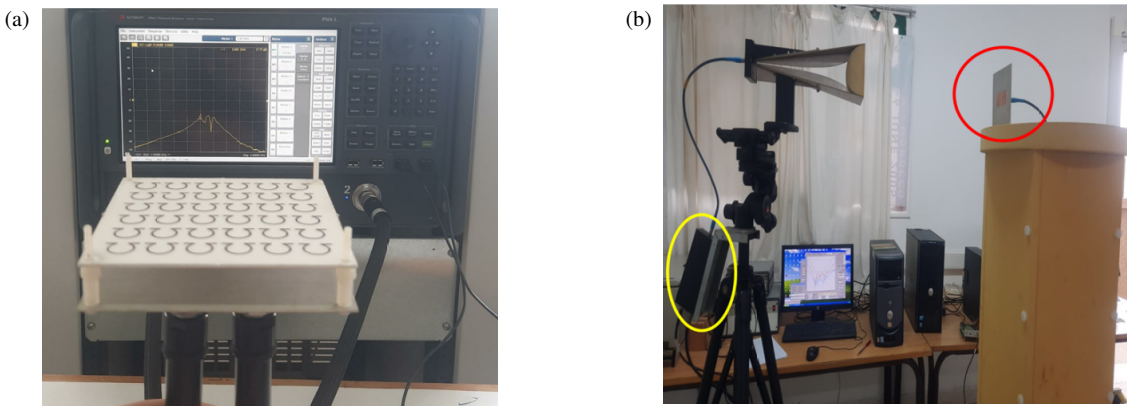

FIGURE 15. (a) VNA network. (b) Measured of radiation pattern.

Figure 12 presents the simulated and measured realized gains of the proposed antenna array with and without the metasurface around the resonance frequency of 2.85 GHz and shows a good agreement. It can be observed that the introduction of the metasurface enhances the realized gain of the antenna structure by 2.3 dB.

Figures 13 and 14 present the measured and simulated radiation patterns of the antenna array structure in the E-plane and H-plane when Antenna 1 and Antenna 2 are excited separately at 2.85 GHz. From Figs. 13 and 14, it can clearly be seen that the measured and simulated results exhibit strong agreement. Moreover, the introduction of the metasurface enhances the radiation performance by improving directivity, lowering sidelobe levels, and increasing pattern symmetry between the two ports. This improvement confirms the role of the metasurface in controlling surface wave propagation and reducing mutual coupling effects.

TABLE 2. Comparison of the proposed method with the referenced antennas.

Ref.	Method	Freq. (GHz)	$\lvert S_{21}\rvert$	E-E (λ_0)	Height (λ_0)	Eff (%) Improvement
[5]	MAAD	5.6	-25	0.06	0.05	20
[6]	MAAD	5.8	-20	0.02	0.12	16
[7]	EBG	5.8	25	0.06	0.05	15
Pro.	MAAD	2.85	-15	0.06	0.14	24

To clearly emphasize the contributions of our work, Table 2 summarizes a comparison of the proposed closely coupled antennas based on metasurfaces with state-of-the-art decoupling antenna designs. This table includes key parameters such as isolation, efficiency, and edge-to-edge distance, and covers different methods like MAAD and the EBG structure. This work improves the efficiency by 24% and reduces the mutual coupling by up to -50 dB within the operating frequency band.

From Table 2, it is clear that our design offers good isolation and improved radiation efficiency compared to other antenna designs proposed in the literature. It is worth noting that, for isolation, Table 2 presents the value at the resonance frequency. However, as shown in Fig. 11, the isolation exceeds 50 dB around 2.9 GHz.

4. CONCLUSION

This paper introduces a method for reducing mutual coupling in a MIMO antenna system using an omega-shaped metasurface. Measurement results demonstrate a 50 dB improvement in isolation at 2.85 GHz, representing a significant reduction in coupling between the antennas. Furthermore, the gain is enhanced by 2.3 dB. We have also observed that the efficiency is enhanced by 30% through the utilization of the metasurface, and the envelope correlation coefficient (ECC) improves from 0.01 to 0.0001 at the resonance frequency of 2.85 GHz, respectively. Owing to these results, the proposed work is relevant for 5G sub-6 GHz MIMO handsets, IoT devices, and compact base-station antennas, where enhanced isolation and preserved radiation efficiency are critical.

ACKNOWLEDGEMENT

This work was financially supported in part by the Spanish Government under the grant PID2024 158965OB-C22 funded by MICIU/AEI/10.13039/501100011033, and by the Contrato Programa Gobierno de Cantabria-UC under Proyectos Puente 2024 funds, under the grant 12.VP96.64662.

REFERENCES

[1] Jensen, M. A. and J. W. Wallace, "A review of antennas and propagation for MIMO wireless communications," *IEEE Transactions on Antennas and Propagation*, Vol. 52, No. 11, 2810–2824, 2004.

[2] Duggani, L., U. Naik, and V. Rayar, "Review of mutual coupling reduction in microstrip patch antenna array for MIMO applications," in *2020 3rd International Conference on Intelligent Sustainable Systems (ICISS)*, 1227–1231, Thoothukudi, India, 2020.

[3] Chen, X., S. Zhang, and Q. Li, "A review of mutual coupling in MIMO systems," *IEEE Access*, Vol. 6, 24 706–24 719, 2018.

[4] Larsson, E. G., O. Edfors, F. Tufvesson, and T. L. Marzetta, "Massive MIMO for next generation wireless systems," *IEEE Communications Magazine*, Vol. 52, No. 2, 186–195, 2014.

[5] Wang, Z., L. Zhao, Y. Cai, S. Zheng, and Y. Yin, "A meta-surface antenna array decoupling (MAAD) method for mutual coupling reduction in a MIMO antenna system," *Scientific Reports*, Vol. 8, No. 1, 3152, 2018.

[6] Wang, Z., C. Li, and Y. Yin, "A meta-surface antenna array decoupling (MAAD) design to improve the isolation performance in a MIMO system," *IEEE Access*, Vol. 8, 61 797–61 805, 2020.

[7] Wang, Z., C. Li, Q. Wu, and Y. Yin, "A metasurface-based low-profile array decoupling technology to enhance isolation in MIMO antenna systems," *IEEE Access*, Vol. 8, 125 565–125 575, 2020.

[8] Guha, D., S. Biswas, M. Biswas, J. Y. Siddiqui, and Y. M. M. Antar, "Concentric ring-shaped defected ground structures for microstrip applications," *IEEE Antennas and Wireless Propagation Letters*, Vol. 5, 402–405, 2006.

[9] Pan, B. C., W. X. Tang, M. Q. Qi, H. F. Ma, Z. Tao, and T. J. Cui, "Reduction of the spatially mutual coupling between dual-polarized patch antennas using coupled metamaterial slabs," *Scientific Reports*, Vol. 6, No. 1, 30288, 2016.

[10] Alibakhshikenari, M., F. Babaeian, B. S. Virdee, S. Aïssa, L. Azpilicueta, C. H. See, A. A. Althuwayb, I. Huynen, R. A. Abd-Alhameed, F. Falcone, and E. Limiti, "A comprehensive survey on "Various decoupling mechanisms with focus on metamaterial and metasurface principles applicable to SAR and MIMO antenna systems"," *IEEE Access*, Vol. 8, 192 965–193 004, 2020.

[11] Jaouad, S., I. Hammouchi, M. Khalladi, O. El Mrabet, and M. Aznabet, "Enhanced coupling and bandwidth in MIMO system antenna based on dielectric resonator antenna using metasurface," in *2024 International Microwave and Antenna Symposium (IMAS)*, 1–4, Marrakech, Morocco, 2024.

[12] Tang, G., T. Xiao, L. Cao, R. Cheng, C. Liu, L. Huang, and X. Xu, "A multi-frequency low-coupling MIMO antenna based on metasurface," *Electronics*, Vol. 13, No. 11, 2146, 2024.

[13] Wu, T. and L. Yan, "High isolation circularly polarized MIMO antenna based on metasurfaces," *iScience*, Vol. 27, No. 9, 110749, 2024.

[14] Khadar, S. A. and S. Sahu, "A tri-band CP MIMO antenna influenced by metasurface for next generation wireless communication," *Journal of Electromagnetic Waves and Applications*, Vol. 39, No. 15, 1794–1823, 2025.

[15] Pfeiffer, C., C. Zhang, V. Ray, L. J. Guo, and A. Grbic, "High performance bianisotropic metasurfaces: Asymmetric transmission of light," *Physical Review Letters*, Vol. 113, No. 2, 023902, 2014.

[16] Saadoun, M. M. I. and N. Engheta, "A reciprocal phase shifter using novel pseudochiral or ω medium," *Microwave and Optical Technology Letters*, Vol. 5, No. 4, 184–188, 1992.